Applied Catalysis A: General xxx (2015) xxx–xxx

Contents lists available at ScienceDirect

Applied Catalysis A: General

journal homepage: www.elsevier.com/locate/apcata

Impregnated Ni/ZrO_2 and Pt/ZrO_2 catalysts in dry reforming of methane: Activity tests in excess methane and mechanistic studies with labeled $^{13}CO_2$

Miklós Németh[a], Zoltán Schay[a], Dávid Srankó[a], Johanna Károlyi[a], György Sáfrán[b], István Sajó[c], Anita Horváth[a,*]

[a] Institute for Energy Security and Environmental Safety, Centre for Energy Research, Konkoly-Thege M. street 29-33, H-1121 Budapest, Hungary
[b] Institute for Technical Physics and Materials Science, Centre for Energy Research, Konkoly-Thege M. street 29-33, H-1121 Budapest, Hungary
[c] University of Pécs, Szentágothai Research Centre, Ifjúság street 20, H-7624 Pécs, Hungary

ARTICLE INFO

Article history:
Received 13 December 2014
Received in revised form 1 April 2015
Accepted 5 April 2015
Available online xxx

Keywords:
Mechanism of dry reforming
Ni/ZrO_2
Pt/ZrO_2
Circulation system
DRIFTS
Coke formation
$^{13}CO_2$ isotope labeled experiments

ABSTRACT

In the present work, 1%Ni/ZrO_2, 3%Ni/ZrO_2 and 1%Pt/ZrO_2 catalysts prepared by impregnation with the concomitant addition of $NaHCO_3$ were investigated and compared by structural investigations such as TEM, XRD, TPR, XPS and DRIFTS methods. Temperature programmed dry reforming (DRM) experiments were done (i) at atmospheric pressure in plug flow reactor and an in situ DRIFTS cell or (ii) under sub atmospheric pressure (~50 mbar) in a closed loop circulation system using labelled $^{13}CO_2$ to trace the fate of carbon compounds. The calcined and reduced fresh catalysts contained nanoparticles in the range of 2–18 nm. According to the TPR results, in 3%Ni/ZrO_2 catalyst most of Ni is in strong interaction with the support. The presence of sodium was suggested to induce the appearance of strongly bound bridged CO sites during CO chemisorption in DRIFTS measurements for all samples and to cause BE shift in XPS spectrum of the highly dispersed Pt/ZrO_2 only. In the catalytic tests in plug flow reactor the 3 wt%Ni/ZrO_2 sample turned to be the most active catalyst, but coke was deposited on its surface measured by the subsequent temperature programmed oxidation (TPO) measurements. In situ low temperature DRIFTS-DRM measurements suggested that stability of surface carbonates is less when dispersed electron-rich Pt nanoparticles are on the ZrO_2 support, while more carbonates accumulate on Ni/ZrO_2 samples. Based on our isotope labeled $^{13}CO_2 + {}^{12}CH_4$ experiments in circulation system, the same initial reaction pathways could be suggested for the Ni and Pt catalysts. The reactive surface carbon species from the two different sources (CH_4 and CO_2) were completely scrambled on 3 wt%Ni/ZrO_2 at 600 °C, suggesting that common reaction intermediates do exist.

1. Introduction

Climate change and depletion of hydrocarbon resources of the Earth are the main causes of the nowadays increased research on CO_2 (dry) reforming of methane, which yields syngas with equimolar ratio of CO and H_2. The reaction is strongly endotherm, high temperature is necessary to reach the desired conversion. Although supported noble metals (e.g.: Ru, Rh, Pt) as catalysts show high conversion, nickel would be a more suitable choice because of its lower price and higher abundance. Unfortunately, carbon deposits more readily form on nickel than on noble metal surfaces during the reaction leading usually to fast deactivation of the catalyst [1–3]. Depending on the reaction parameters, beside the main dry reforming reaction [1], the following most important side reactions can occur:

$$CH_4 + CO_2 \leftrightarrow 2CO + 2H_2 \qquad \Delta H^\circ_{298\,K} = 247\,kJ/mol \tag{1}$$

$$CH_4 \leftrightarrow C + 2H_2 \qquad \Delta H^\circ_{298\,K} = 75\,kJ/mol \tag{2}$$

$$CO_2 + H_2 \leftrightarrow CO + H_2O \qquad \Delta H^\circ_{298\,K} = 41\,kJ/mol \tag{3}$$

$$2CO \leftrightarrow C + CO_2 \qquad \Delta H^\circ_{298\,K} = -171\,kJ/mol \tag{4}$$

$$CO + H_2 \leftrightarrow C + H_2O \qquad \Delta H^\circ_{298\,K} = -131\,kJ/mol \tag{5}$$

Side reactions that involve changing of CO concentration are the reverse water–gas shift (RWGS, [3]), Boudouard reaction [4], reverse carbon gasification reaction [5]. Beside the last two,

* Corresponding author. Tel.: +36 13922222.
E-mail address: horvath.anita@energia.mta.hu (A. Horváth).

http://dx.doi.org/10.1016/j.apcata.2015.04.006
0926-860X/

methane cracking reaction [2] can deposit surface coke. Depending on the temperature and concentration of reactants, the RWGS reaction may proceed forward or backward direction since its equilibrium constant is close to 1 within the overall temperature interval of dry reforming [4].

The mechanism of the reaction was widely studied, still, apparent contradictions arose between the results, and it seems that depending on the reaction conditions, support material, and active metal, the suggested elementary steps and also the rate determining step are often not the same [5–8]. The basic view of the reaction mechanism is that methane dissociates on the metal surface, and CO_2 can be activated on the support [9,10], at the metal–support interface [5,11] or even on the metal surface [8,10]. The surface CH_x fragments or surface C species react with active O or OH species and desorb as CO and H_2 product [12]. One of the key steps is the activation/dissociation of methane on the catalytically active metal surface, that was claimed to be irreversible in some cases [8,13] and reversible in others [7,14]. If the CH_x intermediates thus formed convert to elemental carbon that cannot be – for any reason – gasified, coke deposition takes place, nanotubes or graphitic layers around the metal particles form.

The significant coke deposit can still leave the catalyst work as it was seen in many references [15–18]. Carbon nanotube formation is structure sensitive and it is greatly suppressed when metal particles are small enough ($d < 25$ nm) [19]. High dispersion of the active metal can be achieved by choosing an appropriate support material, which stabilizes the metal nanoparticles via strong interaction such like Pt on ZrO_2 support [7]. The other way to reduce coke formation is to increase the concentration of active oxidants via (i) applying reducible supports such as CeO_2 with high oxygen mobility [15] or (ii) enhancing the CO_2 adsorption/activation step by using basic supports[6,13,20,21] or (iii) adding alkaline K, CaO promoters to the (acidic) support [9,10,22,23]. Thus, CO_2 either forms carbonates that scavenge carbon from Ni surface at the perimeter sites [10] or dissociates at the metal–oxide interface where oxygen vacancies are abundant due to the presence of a promoter [5]. Sodium is considered to be a promoter for dry reforming. Lovell et al. [16] pointed out that Na addition to Ni/MCM-41 caused lower activity, did not change basicity but decreased the acidity, and the RWGS was prevalent at all Ni loadings. Stability increase was seen by Ballarini et al. upon Na addition to Pt/ZrO_2 due to the creation of basic sites [23], but the positive effect of sodium species was observed on Pt/Al_2O_3 only above 0.5 wt% Pt content [22].

In our laboratory several aspects of dry reforming have been already investigated over Ni-based catalysts prepared by different methods and supported on $MgAl_2O_4$ and Ce-Zr-oxides [15,20,21]. The aim of the present study was to use ZrO_2 support material and the same amount of sodium as catalyst promoter for the synthesis of supported Ni and Pt catalysts, applying a simple preparation method that could be feasible at larger (industrial) scale. Differences between the samples were studied by XRD, TEM, XPS, DRIFTS methods and catalytic behavior was evaluated in plug flow reactor with high excess of methane and in closed loop circulation system at sub atmospheric pressure with labeled $^{13}CO_2$ reactant to be able to trace the fate of different carbon species on the catalyst surface.

2. Experimental

2.1. Sample preparation

Zr-hydroxide from MEL Chemicals was calcined at 600 or 800 °C resulting ZrO_2 with 37 and 22 m^2/g surface area, respectively. Accordingly, support denotation Zr6 or Zr8 reflects the 600 or 800 °C calcination temperature. Preparation of catalyst samples was done by impregnation technique at 70 °C with large amount of excess water, using 19.3 mM H_2PtCl_6 or 150 mM $Ni(NO_3)_2$ solutions to yield 1 wt% Pt (Zr8Pt1imp) and 1 wt% (Zr8Ni1imp) or 3 wt% Ni (Zr6Ni3imp) in the final catalysts. To support 3 wt% Ni loading, ZrO_2 calcined at 600 °C was used in order to have higher surface area to better accommodate the more Ni. The initial pH during the impregnation was set to pH 6.5 with $NaHCO_3$ that served also as source of Na promoter to yield about 0.6 wt% Na in the final catalysts. The water was slowly evaporated during 3–4 h, then the solid was dried. Dried samples were calcined in air at 600 °C and reduced in H_2 at 600 °C for 2 h and stored in air before further use (these are referred as the as received samples from now on).

2.2. Catalyst characterization

Metal and Na content of Zr8Ni1imp sample was ascertained by Prompt Gamma Activation Analysis (PGAA), otherwise, nominal values were taken for the two other samples.

The phase composition of crystalline components of the calcined/reduced samples was investigated by X-ray powder diffraction (XRPD) analyses. The diffraction patterns were obtained in a Philips model PW 3710 based PW 1050 Bragg-Brentano parafocusing goniometer using Cu Kα radiation ($\lambda = 0.15418$ nm), graphite monochromator and proportional counter. The digitally recorded XRD scans were evaluated for quantitative phase composition using a full profile fit method with corrections for preferred orientation and microabsorption.

The elemental composition of the samples, morphology and structure of the metal particles were studied by transmission electron microscopy (TEM). The TEM samples were prepared by drop drying the aqueous suspensions on carbon-coated micro grids. The particle size distribution and the local elemental composition were obtained by means of a conventional Philips CM20 transmission electron microscope (TEM) operating at 200 kV equipped with a Bruker energy dispersive spectrometer (EDS) for electron probe microanalysis. Average particle size of Zr8Pt1imp was given by counting about 300 particles. High resolution transmission electron microscopic investigations (HRTEM) were carried out by a JEOL 3010 microscope operating at 300 kV with point resolution of 0.17 nm.

Reduction properties of the reoxidized Ni samples were investigated in Micromeritics AutoChem 2920 catalyst characterization system in 10%H_2/Ar stream with 10 °C/min temperature ramp up to 700 °C using 50 mg catalyst. TCD response was calibrated in a separate measurement before the TPR run. Reducibility of the samples was determined by quantification of H_2 consumption supposing that NiO was reduced during the TPR.

For the determination of surface composition, X-ray photoelectron spectroscopy measurements were applied using a KRATOS XSAM 800 XPS machine equipped with an atmospheric reaction chamber. Al Kα characteristic X-ray line, 40 eV pass energy and FAT mode were applied for recording the XPS lines of Ni 2p, Pt 4f, C 1s, O 1s, Zr 3d, Cl 2p, Na 1s and Na 2s. C 1s binding energy at 285.0 eV was used as reference for charge compensation. The samples were measured in as received state and after calcination in synthetic air at 600 °C for 30 min (10 °C/min), followed by a hydrogen-treatment in H_2 at 600 °C for 30 min (10 °C/min).

In situ diffuse reflectance infrared Fourier transform spectroscopy (DRIFTS) was applied to study the catalyst samples under different conditions. Spectra were collected on a Nicolet is50 infrared spectrometer equipped with a MCT detector and a Specac DRIFT accessory and environmental chamber with a ZnSe window. The maximum allowed temperature of the cell was 500 °C. The sample in the cell was contacted with the gas atmosphere flowing in and out of the cell but the gas stream did not flow through the catalyst powder, and so this arrangement does not correspond to a plug flow reactor. Spectra were obtained by collecting 64 scans

Please cite this article in press as: M. Németh, et al., Appl. Catal. A: Gen. (2015), http://dx.doi.org/10.1016/j.apcata.2015.04.006

with a resolution of 4 cm^{-1} and presented as ln(1/*R*) mode, where *R* is reflectance. For in situ reduction, the sample holder of DRIFTS cell was fully loaded with the catalyst powder, then heated to 500 °C in 5% H_2/Ar atmosphere with 10 °C/min rate and kept at this temperature for 30 min, then it was cooled to the desired temperature of the measurement. CO chemisorption measurements at room temperature were done using 1% CO in He. Temperature programmed desorption (TPD) of the adsorbed CO was followed in Ar. Temperature programmed DRIFTS-DRM reaction was conducted in the DRIFT cell with CH_4:CO_2 = 70:30 reactant mixture (flow rate: 50 cm^3/min) up to 500 °C, then, after a 30 min hold time the sample was cooled down in the reaction mixture (to 100 °C for the Zr8Pt1imp sample and to 300 °C for the Zr6Ni3imp sample), and finally, TPD in Ar was carried out up to 450 °C.

2.3. Catalytic measurements

2.3.1. Catalytic and TPO measurements in plug flow reactor

Catalytic tests were done in a fixed-bed plug flow reactor at 1 atm using CH_4:CO_2:Ar = 68:31:1 mixture (from now on this is referred as DRM mixture for the sake of simplicity). It should be pointed out that this particular reagent gas mixture was chosen to mimic the composition of some natural gas wells in Hungary. 30 mg (Zr8Pt1imp, Zr8Ni1imp) or 10 mg (Zr6Ni3imp) of catalyst along with 100 mg of diluting quartz beads were placed in a tubular quartz reactor where the reactant mixture at a flow rate of 20 ml/min (40 or 120 l/h/g_{cat}) was introduced. Before the catalytic measurements the as received samples were in situ reduced in 30 ml/min H_2 stream at 600 °C for 30 min, with a the temperature ramp of 10 °C/min. After reduction, the sample was purged with He flow (30 ml/min) while it cooled down. Next, the He flow was changed to the reactant gas mixture and temperature was increased to 600 °C with 10 °C/min followed by a 2 h hold time. A quadrupole Pfeiffer Prisma mass spectrometer was used for analysis connected via a differentially pumped quartz capillary to the reactor outlet. Due to the reaction stoichiometry – that causes mass flow increase at the outlet of the reactor – argon was used as an internal reference gas for calculation of the outlet mass flows, to determine CO/H_2 ratio as well as methane and carbon dioxide conversion values, after adequate calibration.

The quantitative analysis was based on the following equation:

$$f_x \times \frac{I_x}{I_{Ar}} = \frac{F_x}{F_{Ar}}$$

where F_x = gas mass flow rate (x = CH_4, CO_2, CO or H_2);
F_{Ar} = mass flow rate of argon;
I_x = mass signals (x = CH_4^+, CO_2^+, CO^+, H_2^+);
f_x = calibration factor for each individual gas component.

The following mass signals as representatives of the gas components were measured: 2-H_2, 15-CH_4, 28-CO, 44-CO_2. In quantification of mass signal m/e = 28 (CO), the actual fragmentation of m/e = 44 (CO_2) was taken into account. The carbon balance in the effluent was between 95% and 102% in all measurements. The relative difference between two repeated catalytic runs was a maximum of 5%. Thermodynamic equilibrium calculations for the special 70%CH_4 + 30%CO_2 composition were carried out with HSC Chemistry program.

Temperature programmed oxidation (TPO) measurements were conducted in the same flow system to detect and measure carbon deposits formed in the DRM reaction. After the catalytic run the samples were calcined in situ in 30 ml/min O_2:He:Ar = 10:89:1 mixture by heating from ambient temperature to 600 °C at a rate of 10 °C/min followed by a 30 min isothermal step. CO_2 signal

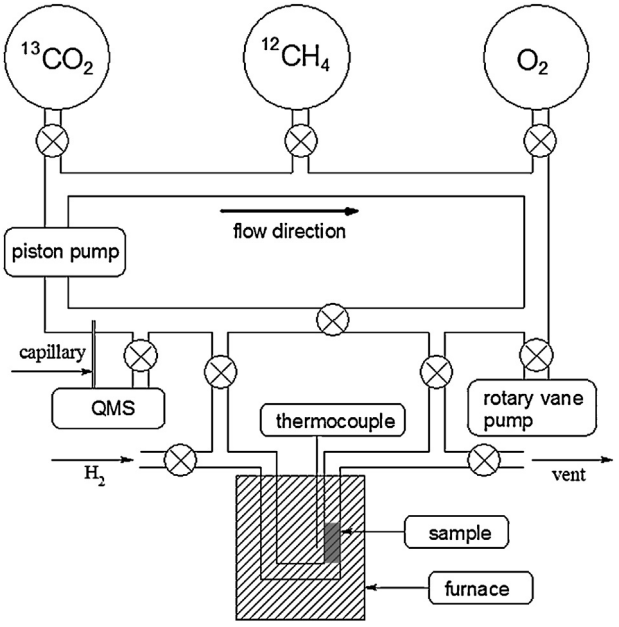

Scheme 1. Schematic diagram of the circulation system (stirred tank reactor) used in $^{13}CO_2$-labeled experiments.

obtained with the mass spectrometer was used for quantification of coke after similar calibration procedure as above.

2.3.2. Catalytic, TPD and TPO measurements at sub atmospheric pressure in a closed loop circulation system using $^{13}CO_2$

An all-glass circulation system (shown in Scheme 1) was applied to conduct isotope-labelled reactions at $p \ll 1$ atm pressure. The system could be separated into the gas blending space and the reactor space, and these two could be merged when needed. Reactants were introduced by measuring the sequential pressure with a capacitive pressure gauge during the admission into the gas blending space. Circulation was carried out by a home-made double-acting piston pump. During the DRM reaction and the TPO measurements, the overall system containing certain amount of gases (p = 50 and 200 mbar, respectively) was connected through a fine glass capillary to a Pfeiffer Prisma mass spectrometer and the system functioned as an integral reactor. During the TPD experiments in vacuum, the reactor worked in differential mode, because by opening a by-pass stopcock, the system was pumped down directly by the turbomolecular pump of QMS and so the desorbing species in the vacuum could be directly detected.

DRM experiments in this circulation system are able to provide only qualitative results, due to the nature of the capillary inlet system and the significant pressure increase during the reaction, which would make the MS calibration of all components extremely difficult. As it is known, for some mass numbers the total intensity of the detected ion current is determined by superimposition of the contributions made by various fragment ions originating from different gas components. Only the signals of H_2O and H_2 are free of other components' fragments, when – at higher conversion – labeled and unlabeled carbon compounds are present in the reaction mixture. Considering this uncertainty, still valuable information can be gained via our experiments. Here, the following mass signals were taken as the representatives of the gas components: 2-H_2, 15-CH_4, 17-$^{13}CH_4$, 28-CO, 29-^{13}CO, 44-CO_2, 45-$^{13}CO_2$.

At the beginning of experiments, 30 mg of the sample was placed into a U-shaped quartz reactor tube that could be heated up to 600 °C. In these circulation type experiments, 1:1 ratio of the reactants was used (and not excess methane as in the plug flow

Table 1
Metal content and metal particle size in as received state.

Sample	Me content (wt%)	d_{TEM} (nm)	d_{XRD} (nm)
Zr8Pt1imp	1[a]	1.9 ± 0.3	110
Zr8Ni1imp	1.01[b]	n.a.	11
Zr6Ni3imp	3[a]	n.a.	18

[a] Nominal value.
[b] Ni and 0.7 wt% Na content was measured by PGAA.

tests). After an in situ reduction treatment in H_2 flow at 600 °C for 30 min, sample was cooled to 150–200 °C and evacuated to about 1.5×10^{-2} mbar pressure, then, the premixed 25 ± 0.5 mbar CH_4 and 25 ± 0.5 mbar $^{13}CO_2$ (99% purity, producer: Consigour Ltd.) mixture was admitted onto the evacuated catalyst. Temperature was ramped up to 600 °C with 10 °C/min rate and was hold there for 30 min. In the subsequent step, the sample was cooled to about 200 °C in the gas mixture present, then evacuated and temperature programmed desorption of the surface species retained was carried out with increasing the temperature back to 600 °C and hold there for 30 min. In this TPD mode the above mentioned by-pass stopcock was opened and so the small amount of desorbing components could be measured with increased sensitivity compared to the case when the capillary route was used. Finally, oxidation of the remaining surface coke after the TPD experiment was done as follows. TPO measurements were carried out by adding 200 mbar oxygen to the evacuated catalyst at room temperature, and ramping the temperature again to 600 °C. The CO_2 signal during TPO experiments was calibrated, and the surface coke evolving as gas phase CO_2 was quantified.

3. Results and discussion

3.1. Catalyst characterization

Table 1 contains the metal particle size of the samples obtained by XRD and/or TEM. Fig. 1a–c depicts the XRD patterns of the samples. Results showed that the oxide support calcined at 600 °C has ZrO_2 particles of 38 nm while the one calcined at 800 °C contains 66 nm size oxide particles. XRD could provide limited information about the size of Ni particles, because the metal content was low, and the particles were relatively small, moreover, the Ni (1 1 1) and the monoclinic baddeleyite ZrO_2 peaks fully overlapped. According to the XRD results, the size of the Ni particles is below 20 nm in both Ni samples and the low loaded catalyst contains the smaller Ni particles (about 11 nm) in as received state.

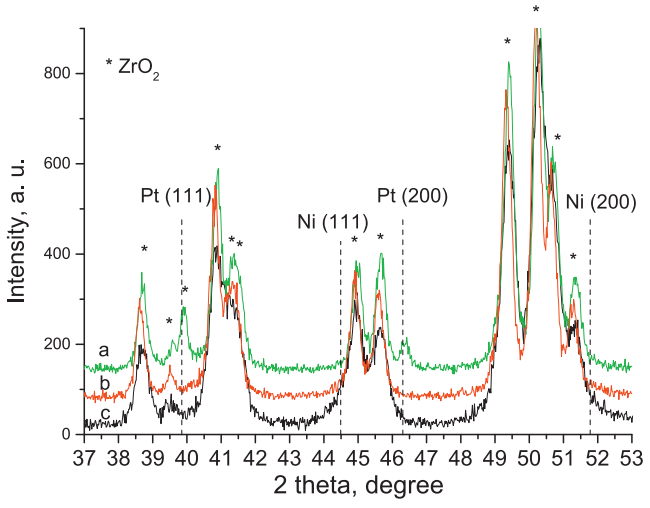

Fig. 1. XRD pattern of the (a) Zr8Pt1imp, (b) Zr8Ni1imp and (c) Zr6Ni3imp catalysts in as received state (after calcination/reduction at 600 °C).

In Fig. 2a, the TEM image of Zr8Ni1imp sample shows that Ni could be detected by EDS analysis along the support in an uneven distribution, but only a few individual Ni particles were able to be discerned among ZrO_2 particles due to the indifferent contrast between the crystalline ZrO_2 support and nickel. If we consider only Zr and Ni components in Zr8Ni1imp the nominal Ni at% (Ni at%= Ni/(Ni + Zr) × 100) is about 2%. As indicated in Fig. 2a, the average Ni content on the measured area shown in the TEM image is 8.2 at%, while the local (marked by the circles) concentrations of Ni vary remarkably as 1.2, 9.1 and 37.4 at% suggesting somewhat inhomogeneous Ni distribution and/or Ni particle size distribution (as TPR results suggested, see later). As for the Pt sample, highly dispersed, typically 2 nm size particles were found well distributed on the ZrO_2 surface. Fig. 2b shows that ZrO_2 support particles (medium gray) are evenly mottled by the small Pt particles (dark gray; some of them marked with arrows). The high resolution TEM image, the magnified insets and the Fast Fourier Transform of the insets in Fig. 2c identify particles with resolved Pt (1 1 1) lattice period of d = 0.227 nm. As revealed by TEM, there was no sign of larger particles, while XRD detected presence of 110 nm sized Pt. This is an apparent contradiction, but we should keep in mind that XRD gives volume weighted, TEM data show number weighted average particle size.

Fig. 3 shows the TPR results obtained on the recalcined Ni samples. The measured and theoretical H_2 consumption for Zr6Ni3imp were 26.9 μmol H_2/50 mg_{cat} and 25.6 μmol H_2/50 mg_{cat}, respectively, while for Zr8Ni1imp they were 11.1 μmol H_2/50 mg_{cat} and 8.5 μmol H_2/50 mg_{cat}, respectively. This means that Ni oxide was completely reduced below 600 °C in both samples. There were 2 types of nickel oxide species on Zr8Ni1imp as the 2 overlapping TPR peaks suggested: the NiO which is reduced at around 340 °C is in weak interaction, while the NiO_x species reducible around 490 °C are in strong interaction with the support [24]. The difference between the two catalysts was the ratio of these 2 types of nickel oxide particles/species: on the surface of Zr6Ni3imp most of the nickel oxide was in strong interaction with the support and reduced at around 490 °C.

Table 2 contains the results of XPS investigations. The measurements carried out on as received samples detected Na and some Cl beside Ni and Pt. (The surface Cl/Zr ~ 0.6 ratio – not shown in the table – was about the same in all the samples and did not change significantly after the in situ treatments.). Concerning the Pt sample, the particles were of metallic state as it is seen in Table 2 and Fig. 4a and b. However, after in situ calcination/reduction treatment surface concentration of Pt not only decreased but the binding energy of 4f electrons shifted to lower value. This negative shift together with the increase of surface Na concentration may suggest that strong (electronic) interaction persist in reducing atmosphere between small platinum nanoparticles and the support containing alkali ions [25]. The decrease of Pt/Zr ratio upon reduction may be due to additional sintering or to the decoration of small Pt nanoparticles with ZrO_x [26] or even with alkali patches [27].

As Figs. 5a and 6a show, Ni is mostly oxidic in as received state due to the storage in air, and present as NiO and $Ni(OH)_2$, although the low-loaded Ni sample contains some metallic Ni according to the binding energy value of 853.1 eV that is too low to be purely NiO. Upon in situ reduction in the XPS pretreatment chamber, the amount of the zero valent Ni greatly increased, but $Ni(OH)_2$ species were still detected. The fact that XPS analysis detected Ni^{2+} after reduction may partly reflect the imperfect flow conditions and temperature distribution in the XPS pretreatment chamber during H_2 treatment, but we assume that this is somehow in connection with the presence of sodium species as well. After reduction the Na_2CO_3 on the support in

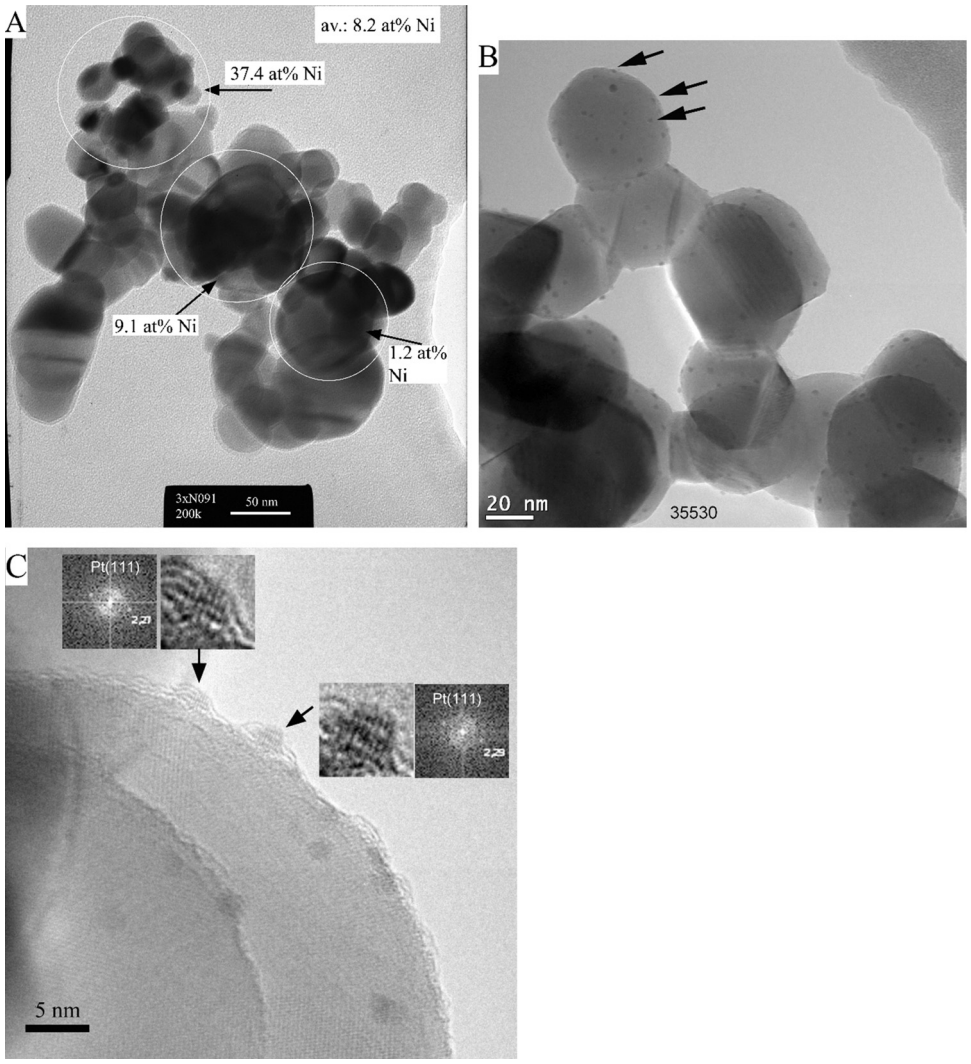

Fig. 2. Results of TEM measurements of the as received catalysts. (a) TEM image of Zr8Ni1imp and Ni content at different places measured by EDS; (b) TEM image of Zr8Pt1imp (a few Pt particles are signed with arrows); (c) HRTEM image of Zr8Pt1imp and the Fast Fourier Transform of the magnified insets identifying particles with resolved Pt (1 1 1) lattice period.

close vicinity of Ni particles may decompose which would produce Ni-hydroxide at the interface of Ni particles. The fraction of metallic Ni was lower on Zr8Ni1imp and a bit higher on Zr6Ni3imp (Figs. 5b and 6b), while Na/Ni = 26.5 was on Zr8Ni1imp and Na/Ni = 16.6 on Zr6Ni3imp. It seems that the higher the Na/Ni ratio the higher the ionic Ni part was detected by XPS experiments. However, we have to keep in mind, that a less significant increase of Na/Zr ratio was seen upon reduction, and no clear shift of binding energies was observed (unlike for Pt sample), probably because of the difference of electronegativities and metal's dispersion.

Next, DRIFTS CO chemisorption measurements were carried out to reveal further differences between the catalysts. Fig. 7 shows the results obtained under 1% CO/He flow at room temperature. Stretching vibration band of linear CO species adsorbed on metal appeared at around 2050 cm^{-1} on Ni samples [28] while at 2085 cm^{-1} on Zr8Pt1imp. In the case of Ni samples there were 2 bands in the bridged CO region at 1930 cm^{-1} and at ~1800 cm^{-1},

Table 2
XPS data of the samples.

Sample	In as received state			After in situ calc/red @600 °C		
	B.E. (eV) $Pt4f_{7/2}$ or Ni $2p_{3/2}$	Surface conc. (at%)		B.E. (eV) $Pt4f_{7/2}$ or Ni $2p_{3/2}$	Surface conc. (at%)	
		Me/Zr	Na/Zr		Me/Zr	Na/Zr
Zr8Pt1imp	70.8 (Pt^0)	0.03	0.16	69.6 (Pt^0)	0.02	0.39
Zr8Ni1imp	853.1 (NiO) 855.9 ($Ni(OH)_2$)	0.05	0.39	852.6 (Ni^0) 856.1 ($Ni(OH)_2$)	0.02	0.53
Zr6Ni3imp	853.8 (NiO) 855.8 ($NiOH)_2$)	0.08	0.71	852.4 (Ni^0) 855.9 ($NiOH)_2$)	0.05	0.83

Please cite this article in press as: M. Németh, et al., Appl. Catal. A: Gen. (2015), http://dx.doi.org/10.1016/j.apcata.2015.04.006

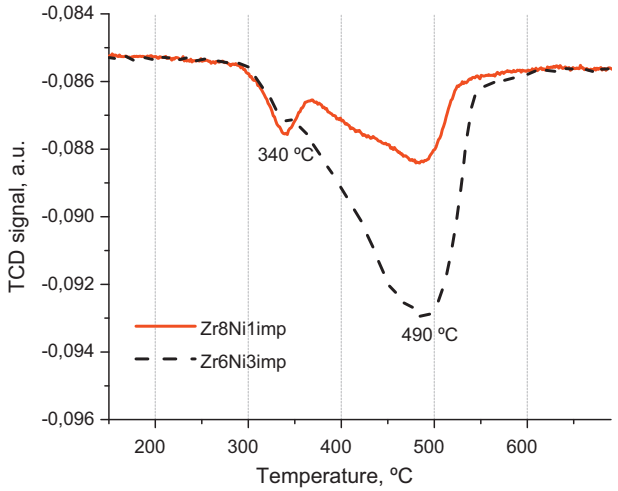

Fig. 3. TPR results after recalcination of the as received samples (conditions: recalcination at 700 °C then TPR in 10%H_2/Ar with 10 °C/min ramp.).

while on the Pt sample only one broad band at around 1800 cm^{-1} could be detected. The linear/bridged CO ratio was significantly larger for the Pt sample (reflecting -partially- its higher dispersion determined by TEM). According to the literature, alkali promotion

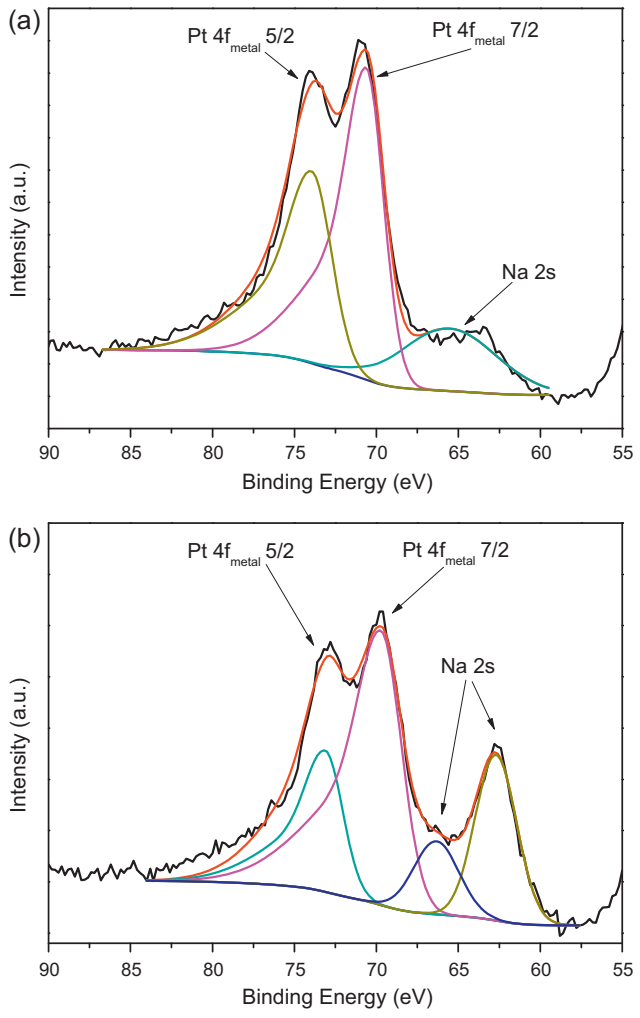

Fig. 4. XPS spectrum of Pt 4f region of Zr8Pt1imp (a) in as received state and (b) after in situ calcination/reduction at 600 °C.

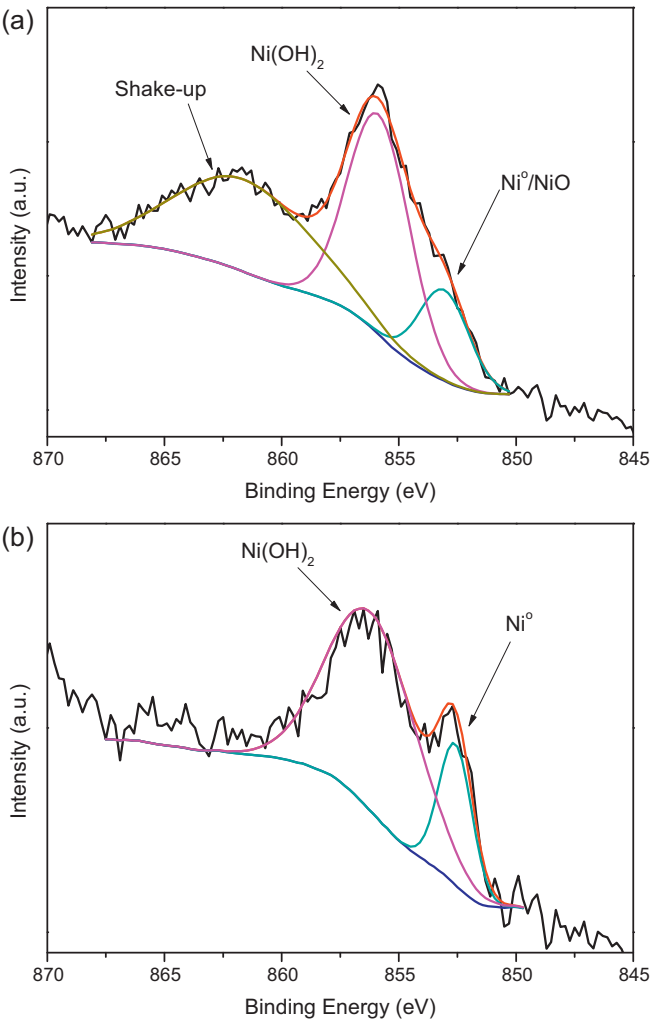

Fig. 5. XPS spectrum of Ni $2p_{3/2}$ region of Zr8Ni1imp (a) in as received state and (b) after in situ calcination/reduction at 600 °C.

can cause formation of new sites with increased electron density, which increases the binding energy of CO to the metal, and weakens the C≡O bond, thus a red shift can be observed in the IR peak positions of adsorbed CO species [29]. Thus, we suggest that the peak at 1800 cm^{-1} could be assigned to CO adsorbed on metal sites that are influenced by sodium or are in close vicinity of sodium, viz. at the metal-support interface. Focusing on the difference between the two Ni samples, we can observe that the ratio of linear CO band to the one at 1800 cm^{-1} is much lower on the Zr8Ni1imp sample than on Zr6Ni3imp. This could be in connection with the observation that on Zr8Ni1imp the surface Na/Ni ratio was higher.

All catalysts showed presence of formate/carbonate species [30] at wavelengths below 1700 cm^{-1} (in higher concentration on Ni-containing samples), while on the pure support (not shown here) no sign of carbonates/formates were seen in the presence of 1% CO/He stream. Sodium via electronic interaction is able to weaken the C≡O bond causing even CO dissociation or carbonate formation [31]. This could be valid in our case as well. During temperature programmed desorption (TPD) of chemisorbed CO in Ar, the linear type CO on Pt was still observable at 400 °C while CO on Ni desorbed at around 300 °C from the Zr6Ni3imp catalyst (not shown for the sake of brevity). This reflects that Pt surface keeps CO adsorbed more strongly than Ni.

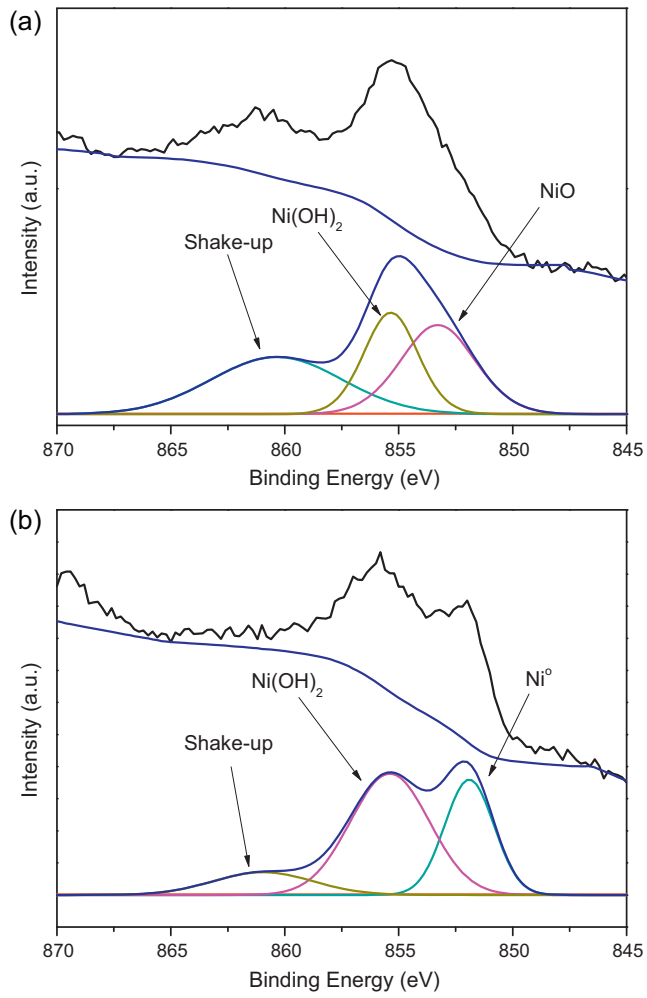

Fig. 6. XPS spectrum of Ni $2p_{3/2}$ region of Zr6Ni3imp (a) in as received state and (b) after in situ calcination/reduction at 600 °C.

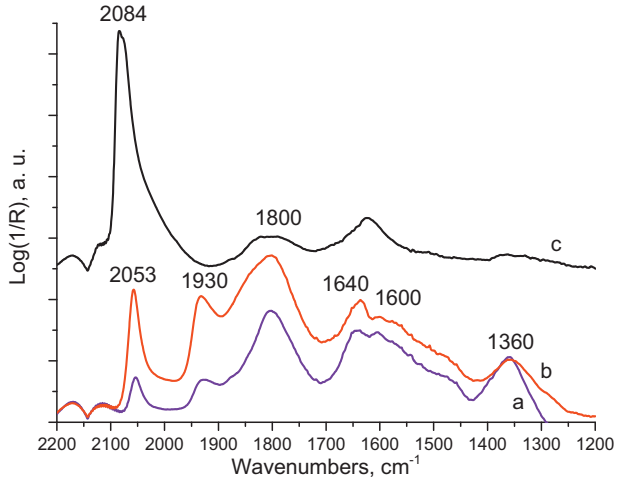

Fig. 7. DRIFTS spectra obtained during CO chemisorption in 1%CO/He mixture at room temperature on (a) Zr8Ni1imp, (b) Zr6Ni3imp and (c) Zr8Pt1imp catalyst. Spectra were corrected with the corresponding spectrum of reduced sample before CO admission.

3.2. Catalytic investigations

3.2.1. DRM tests at 1 atm in plug flow reactor

Catalytic tests in plug flow reactor were carried out with CH_4:CO_2:Ar = 68:31:1 mixture.

Fig. 8a–c shows the summary of catalytic experiments when after in situ reduction at 600 °C in H_2 and cooling in He, the samples were heated up in DRM mixture with 10 °C/min to 600 °C followed by a 2-h-isothermal hold (for Zr8Ni1imp only 1 h). According to the results shown in Fig. 8a, the reaction starts at a bit lower than 400 °C. There is no significant difference between the activities of the samples, but the highest CO_2 and CH_4 conversion is achieved by the Zr6Ni3imp catalyst, and this primacy is maintained at 600 °C for 2 h as well.

At around 450 °C, the ratio of CO_2/CH_4 conversion was the highest for Zr6Ni3imp and the lowest for Zr8Ni1imp with Zr8Pt1imp in between them, but when the temperature reached 600 °C, all samples approached CO_2/CH_4 conversion ratio values of 3. Comparing the catalytic data at the same CH_4 conversion (about 11%), higher CO_2 conversion was needed to get the same amount of CO product on Zr6Ni3imp compared to the two samples, but more H_2 was produced as well, meaning that (partially) dehydrogenated surface carbon species must have been remained on Zr6Ni3imp.

Fig. 8b shows the correlation of the calculated equilibrium concentrations for all measured gas components and the actual concentration values obtained on the most active Zr6Ni3imp sample. The theoretical and the measured values of CO/H_2 ratio versus temperature and time are depicted in Fig. 8c for all the samples. If the CO/H_2 ratio is higher than the theoretical, it is generally considered that beside DRM, reverse water gas shift happens [32]. Actually, water formation was not quantified during the measurements but m/e = 18 signal (H_2O) was fairly low and constant. Higher CO/H_2 ratios were obtained on Zr8Ni1imp and the Pt sample. Ballarini and co-workers [22] experienced that on small Pt particles supported on K- modified Al_2O_3, the RWGS was more pronounced. In the case of Pt, the slight increase of CO_2/CH_4 conversion ratio during the isothermal part could really account for the RWGS, and could reflect some deactivating tendency during the course of reaction [33].

In TPO measurements coke (0.42 mg carbon/mg_{cat} = 68 C/Ni) was removed only form the most active Zr6Ni3imp sample. Despite that coke was formed on Zr6Ni3imp, it had higher activity compared to Zr8Ni1imp. Methane cracking or CO disproportionation was found to be more pronounced when increasing the Ni-loading in Ni/Na-MCM-41 catalyst [16]. Sokolov et al. [5] found that during low temperature DRM (400 °C) the intrinsic activity of Ni/La_2O_3-ZrO_2 grows with Ni particle size and so does the coking rate, because the surface carbon is supposed to diffuse to the metal-support interface to react with the carbonates and this is thought to be the rate limiting step under their conditions. Furthermore, Gennequin et al. [18] when studying Co–Mg–Al mixed oxides experienced that higher Co content resulted in higher coke content and higher DRM activity. The severely coked catalyst was more stable, because graphite was thought to act as CH_x collector and to reduce the residence time of carbon species on the metal surface. The higher activity of our 3%Ni/ZrO_2 sample was probably due to the optimal, medium size Ni particles in strong interaction with the support and the optimal distribution of Na promoter forwarding part of the surface coke far from the active Ni sites.

3.2.2. In situ DRIFTS studies in the presence of DRM mixture

FTIR technique was applied in order to investigate the reactivity of surface carbonate species that are considered to take part in the dry reforming reaction at the Pt-ZrO_2 interface according to the literature. As suggested by Lercher and Bitter [26], CO_2 adsorbs on the support as carbonate, while methane decomposes on the metal. The

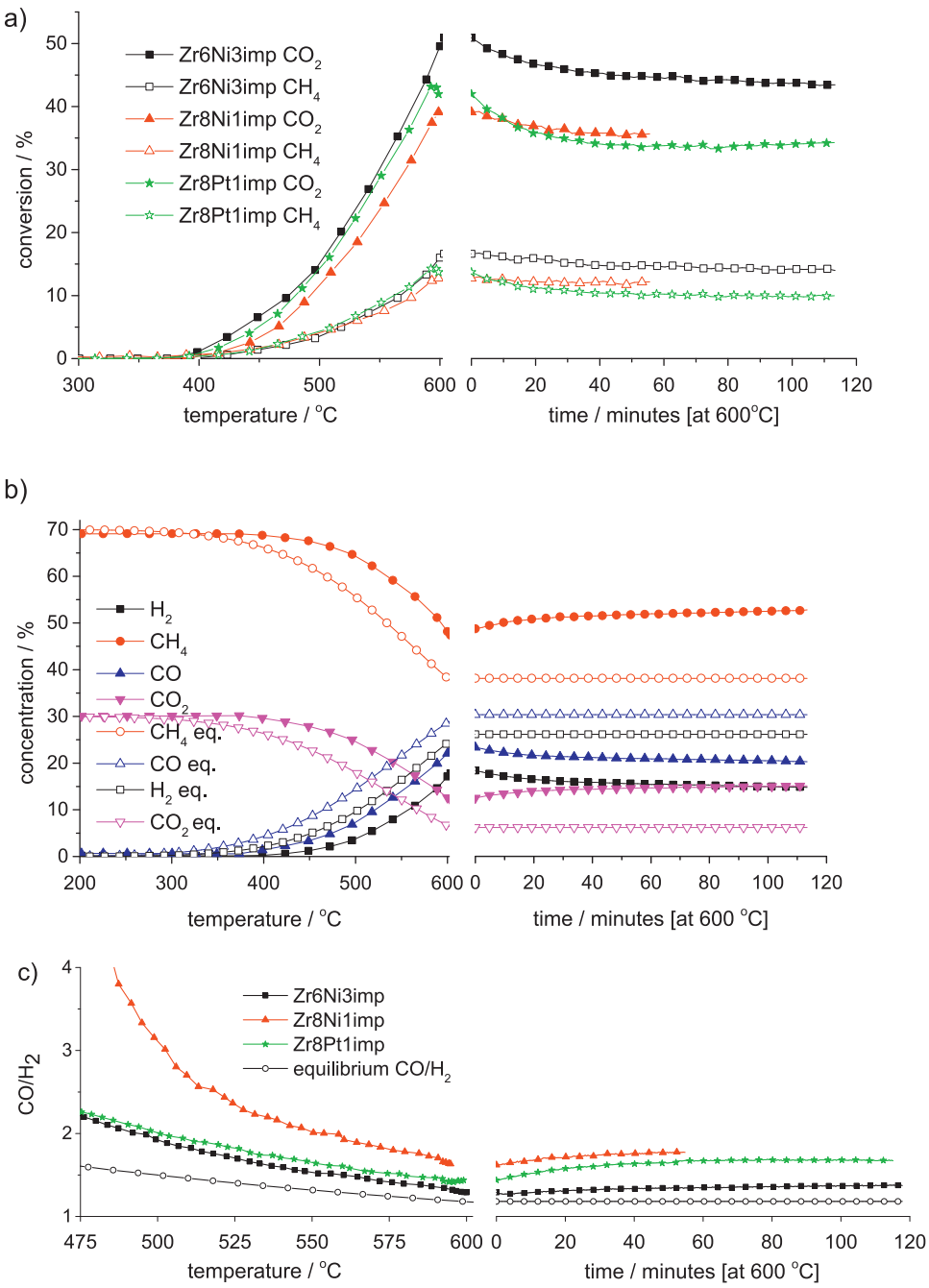

Fig. 8. Results of catalytic tests in plug flow reactor. (a) Conversion values of all samples and (b) concentration values of Zr6Ni3imp compared to the calculated chemical equilibrium composition and (c) CO/H_2 ratio of all samples and the corresponding equilibrium data (conditions: CH_4:CO_2:Ar = 68:31:1, 20 ml/min flow, temperature ramp up to 600 °C then 120 min isothermal hold at 600 °C).

coke species on the metal reduce the carbonate to formate species while CO is formed. The formate decomposes rapidly to OH and CO. Thus, we expected to see changes of surface carbonates in the course of reaction via FTIR technique.

Our catalysts in the DRIFTS cell were contacted with basically the same DRM mixture that was used in the plug flow tests (without 1% Ar). Using very similar conditions (atmospheric pressure, same reactant concentration), we attempted to identify adsorbed species present under our reaction conditions. A main restriction was that the DRIFTS cell could be heated up only to 500 °C, and so the interaction of DRM mixture with the catalysts was studied at maximum 500 °C.

Fig. 9a depicts DRIFTS spectra obtained on Zr8Pt1imp sample in the presence of CH_4:CO_2 = 70:30 mixture ramping the temperature from 25 to 500 °C. The gas phase CH_4 and CO_2 peaks can be easily discerned at wavenumbers of 3015, 1304 and 2360, 2340 cm^{-1}, respectively. At 150 °C, the band at 1630 cm^{-1} splits into 2 broad bands centered at 1680 and 1550 cm^{-1}, which decrease in intensity with temperature rise. The unresolved band at 1630 cm^{-1} could be assigned to the presence of monodentate formates and bidentate bicarbonates, which convert to monodentate bicarbonate and monodentate carbonate above 150 °C. At 200 °C (well before gas phase CO is observed meaning that DRM reaction started) linearly adsorbed CO on Pt appears at 2052 cm^{-1}, and this peak shifts to 2068 cm^{-1} at 500 °C, moreover, at about 1970 cm^{-1} an additional band develops starting from 250 °C. This means that either the adsorbed carbonates decomposed to formates and further to CO, assisted by the oxygen vacancies at the perimeter

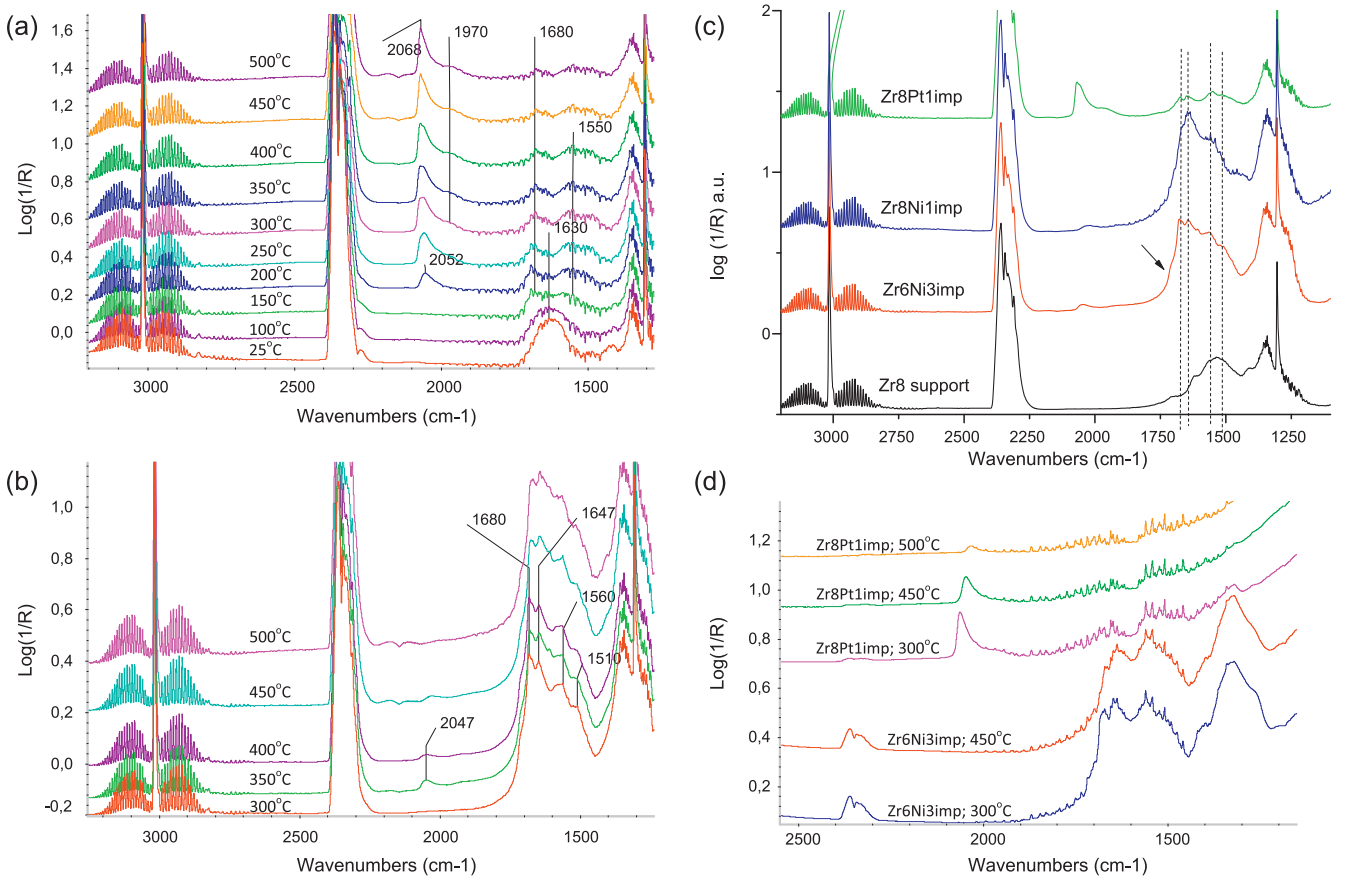

Fig. 9. DRIFTS spectra obtained in the presence of 70%CH_4:30%CO_2 mixture (a) on Zr8Pt1imp sample ramping the temperature from 25 to 500 °C; (b) on Zr6Ni3imp sample ramping the temperature from 300 to 500 °C; (c) comparison of the catalysts at 400 °C (spectra were corrected with the corresponding spectrum of the reduced sample); and (d) DRIFTS spectra taken during Ar-TPD after DRIFTS-DRM experiments on Zr6Ni3imp at 300 and 450 °C; and on Zr8Pt1imp at 300, 450 and 500 °C.

of Pt particles, or gas phase CO_2 dissociation happened on Pt sites, and the CO adsorbed on Pt, furthermore, or all these events could happen. The two bands in the carbonate region are slowly decreasing from 200 to 500 °C while that of the adsorbed CO continuously increases with the appearance of gas phase CO at around 400 °C (start of DRM). The blue shift of the CO band as the temperature increases could also suggest the slight electron density decrease on Pt due to the increased oxygen concentration at the metal–support interface. Based on these results alone, it is not possible to identify the source of CO adsorbed on Pt at different temperatures.

Fig. 9b shows what happens when Zr8Ni3imp is contacted with DRM mixture in the DRIFTS cell and the temperature is increased from 300 to 500 °C. The eye-catching difference here is the tiny peak of linear CO at 2047 cm^{-1} (CO adsorbed to the Ni sites) at 350 °C that even decreases at temperatures close to 500 °C and finally disappears (either chemisorbed CO is not stable enough at that temperature or coke covers the Ni surface). The second difference is the much higher intensity of the carbonates that are positioned in a wide envelope of overlapped peaks at 1680, 1647, 1560 and 1510 cm^{-1} slowly decreasing and restructuring as temperature increases. The peaks detected at 1680 and 1647 cm^{-1} can be assigned to monodentate and bidentate bicarbonates [30]. At 500 °C strong carbonate peaks can be still seen as opposed to the Pt catalyst and ZrO_2 support. This strong carbonate peaks are supposed to be originated form the Na promoter forming Na_2CO_3-like surface species on the support. On well dispersed Pt, the distribution or the effect of Na promoter seems to be different, it is suggested to be partially located on the surface of Pt.

Fig. 9c compares the spectra of all the samples and the ZrO_2 support as well at 400 °C in the presence of DRM mixture. The lower loaded Ni sample possess very similar features as Zr6Ni3imp, only the structure of carbonate peaks is somewhat different and the small shoulder signed on the spectrum of Zr6Ni3imp at about 1710 cm^{-1} assigned to bridged bidentate carbonate[34] is missing here. Concerning the support itself, the peak intensity of adsorbed carbonates is higher on ZrO_2 compared to the Pt/ZrO_2 sample but less intense compared to the Ni/ZrO_2 samples. It seems that the presence of Ni stabilizes the carbonates while Pt destabilizes them, or, the activation of CO_2 is somewhat different on the two metals.

Finally, let us analyze the spectra in Fig. 9d obtained during TPD in Ar flow after the DRM reactions on the best catalysts. The samples were cooled down in the DRM mixture and the gas flow was changed for Ar, then the temperature was increased again. Fig. 9d shows that intense carbonate bands are present up to 450 °C on the Zr6Ni3imp sample, while in the case of Pt sample, desorption of linear CO species and desorption/decomposition of carbonates is seen at 500 °C.

Based on the in situ low temperature DRIFTS-DRM measurements we suggest that reactivity of surface carbonates is much higher when well dispersed Pt electron-rich nanoparticles are on the support, and those nanoparticles are not covered by coke. Most of the carbonates on Ni/ZrO_2 samples do not seem to play a role in the reaction (spectators), and they rather accumulate compared to the pure support. Although, we cannot rule out that some of the carbonates may interact as reaction intermediates, but this could not be seen by DRFITS measurements at temperatures higher than 400 °C, when dry reforming sets really in.

Please cite this article in press as: M. Németh, et al., Appl. Catal. A: Gen. (2015), http://dx.doi.org/10.1016/j.apcata.2015.04.006

3.2.3. Catalytic investigations at sub atmospheric pressure in circulation reactor

Before attempting to understand and describe the reaction mechanism of DRM on these samples, it is worth shortly summarizes the possible elementary steps on ZrO_2 supported metal catalysts. According to the relevant literature [7,35,36], the following steps are the most plausible ones to happen:

$$CO_{2(gas)} \leftrightarrow CO_{ads} + O_{ads} \quad (6)$$

$$CO_{2ads} + H_{ads} \leftrightarrow COOH_{ads} \leftrightarrow CO_{ads} + OH_{ads} \text{ (like RWGS)} \quad (7)$$

$$CO_{ads} \leftrightarrow C_{ads} + O_{ads} \quad (8)$$

$$CH_{4(ads)} \leftrightarrow CH_{x(ads)} + (4-x)H_{ads} \quad (9)$$

$$CH_{xads} + O_{ads} \text{ (or } OH_{ads}) \leftrightarrow CH_xO_{ads} + (H_{ads}) \quad (10)$$

$$CH_xO_{ads} \rightarrow CO_{ads} + \frac{x}{2} H_2 \quad (11)$$

$$COOH_{ads} + H_{ads} \leftrightarrow CHO_{ads} + OH_{ads} \quad (12)$$

$$CH_xO_{ads} + H_{ads} \leftrightarrow CH_4 + H_2O \quad (13)$$

Aparicio et al. [6] according to reactions (7) and (12) supposed that the same intermediate, an aldehyde type CH_xO species forms from both the methane and the CO_2 reactant through the transformation of carbonates-formates.

Now we can focus on the results of temperature programmed DRM reaction conducted with ~25 mbar CH_4 + ~25 mbar labeled $^{13}CO_2$ as it is shown in Fig. 10a–c. On the left *y* axis, the corresponding m/e values are shown versus time (1 MS cycle = 25.8 s), and on the right *y* axis the reaction temperature versus time (=MS cycles) can be followed, which is depicted as a solid line in the figure. As DRM reaction starts, CO (m/e = 28 or 29) and H_2 (m/e = 2) formation can be seen with the concomitant decrease of the mass signal of reactant $^{12}CH_4$ (m/e = 15) and $^{13}CO_2$ (m/e = 45), as expected.

The reaction starts at about 360 °C, and the initial pressure (not shown in the figure) increases to 75 mbar for Zr6Ni3imp and 78 mbar in the case of the other two samples at 600 °C, due to the stoichiometry of reaction. According to Fig. 11, there is a certain temperature (time) delay between the formation of labeled ^{13}CO and unlabeled ^{12}CO, depending on the sample, it is between 60 and 90 °C: first, carbon monoxide originating from carbon dioxide reactant can be detected, and it is in our case the labeled component, ^{13}CO. This is detected the earliest in the case of Zr6Ni3imp, already at 320 °C. It was shown in the literature, that the $CO_2 \leftrightarrow CO$ reaction on the surface of the catalyst is reversible and an order of magnitude faster than the methane dissociation [8,13]. Thus, our experiments are in line with the literature at this point. It is interesting to note (see Fig. 10) that some $^{12}CO_2$ formation can be discerned with a local maximum in its intensity at about 540 °C, which must come from the carbon of unlabeled methane only, and it appears earlier than the ^{12}CO itself derived also from CH_4. This suggests that at the initial state of the reaction, when methane dissociation happens, there is a lot surface oxygen available on the metals and so surface carbon species are totally oxidized to CO_2 with the concomitant desorption of H_2 originating from methane. Later on, ^{12}CO from carbon atoms of methane is produced and when it gets abundant in the gas phase, reversibly adsorbs and transforms to $^{12}CO + O \leftrightarrow {}^{12}CO_2$ on the catalyst, thus, from its first appearance, we can always see some $^{12}CO_2$. It can be concluded that the initial reaction pathways seem to be basically the same for both Ni and Pt samples as Fig. 11 depicts with the same order of product's appearance. The primacy of Zr6Ni3imp sample in dissociating methane at the lowest temperature can be deduced (see the corresponding temperature values in Fig. 11). We should keep in mind that CO on Pt sample is more stable and desorbs at higher temperature than from Ni (see CO chemisorption FTIR measurements), which could influence the apparent order of CO_2 activation.

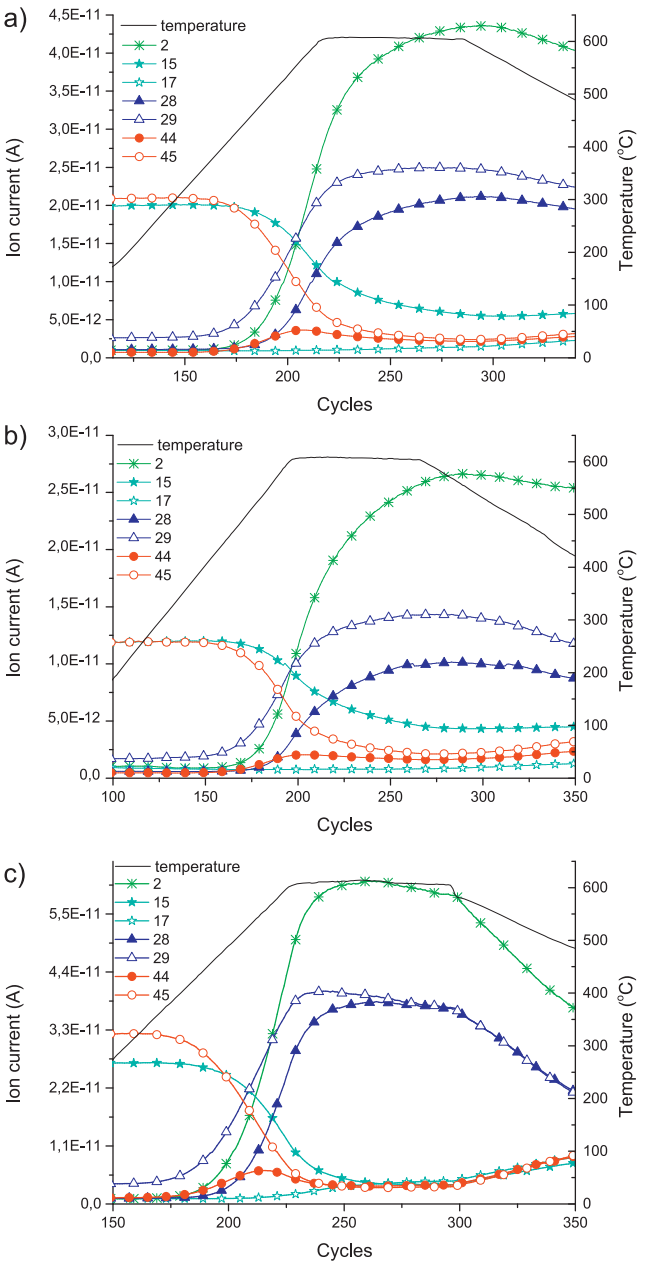

Fig. 10. Dry reforming reaction with 25 mbar CH_4 + 25 mbar $^{13}CO_2$ in circulation system. (a) Zr8Pt1imp, (b) Zr8Ni1imp and (c) Zr6Ni3imp. Conditions: temperature ramp up to 600 °C with 10 °C/min, then 30 min isothermal part, x axis reflects time (1 MS cycle ~ 25.8 s).

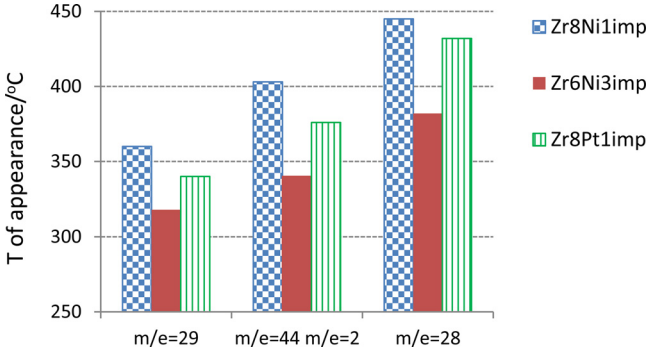

Fig. 11. Initial formation temperatures of ^{12}CO, ^{13}CO, and $^{12}CO_2 + H_2$ during temperature programmed DRM in the circulation system (with 25 mbar CH_4 + 25 mbar $^{13}CO_2$).

Although the quantification of reactant conversions are not provided, it is clearly seen that the reactant $^{13}CO_2$ signal decreases a lot more than methane signal in the case of Zr8Pt1imp (Fig. 10a) and Zr8Ni1imp (Fig. 10b) samples, while both $^{13}CO_2$ and CH_4 concentration (signal) get very low for the Zr6Ni3imp (Fig. 10c) sample, proving that under the present conditions methane transformation is more pronounced on the latter sample. When reaching and maintaining the maximum reaction temperature of 600 °C for 30 min, there is no change in the gas phase concentration for the Zr6Ni3imp sample, this means that the system is close to the equilibrium, while on the two other samples the transformation of reactants apparently continues showing that those systems are still far from equilibrium. We should point out that in the case of Zr6Ni3imp sample, the labeled and unlabeled gas phase CO are in equal quantity at 600 °C. The reactive surface carbon species coming from the two different sources (methane and CO_2) are completely scrambled on Zr6Ni3imp at 600 °C. This is seen when analyzing the curves at the descending temperature side: significant back-reaction ($2CO + 2H_2 \leftrightarrow CO_2 + CH_4$) is detected, the same amount of labeled and unlabeled CO_2 and same amount of labeled and unlabeled CH_4 forms.

We should call one's attention to the fact that some labeled $^{13}CH_4$ (m/e = 17) was produced already at the ascending part of the ramp at 520 °C on Zr6Ni3imp, while less on Zr8Pt1imp and the least and at the latest on Zr8Ni1imp. However, when temperature was finally descending, the formation of labeled methane was observed on all the samples via methanation/back reaction (but to a considerably less extent for the two samples with 1 wt% metal content). The initial $^{13}CH_4$ is suggested to form from the $^{13}C_{ads}$ when the availability of surface oxygen/OH species is restricted but H_{ads} species are abundant; or from gas phase $^{13}CO_2 + H_2$ or $^{13}CO + H_2$ through a common surface intermediate as reaction [6,7] and [12,13] describe.

Johnson and Shamsi [37] observed significant back reaction at 800 °C during isotope labeled flow experiments: using $^{13}CH_4$ flow, $^{13}CO_2$ was detected. Bobin et al. [8] studying DRM on nanocrystalline ceria-zirconia with supported Pt, Ru, Ni, and Ni–Ru particles found no evidence for CO_2 interaction with adsorbed CH_x species or CH_4 activation by carbonates meaning that no common intermediate exist during the reaction. This is not the case here, because the carbon atoms from the reactants are completely mixed in the products at least during/after the isothermal part.

Next, TPD experiments in vacuum were carried out on the samples which were previously cooled down to about 200 °C in reaction mixture and then evacuated. We are aware of that the cooling step in the gas mixture may influence the surface carbon species on the catalyst surface, but according to the results shown in Fig. 12, still differences can be seen among the samples. It is a common observation, that no methane was detected during TPD measurements. From the surface of Zr8Pt1imp sample, only labeled and unlabeled CO_2 (peaks at 280 and 430 °C) and H_2 (peaks at 230 and 520 °C) were desorbed. We should recall that Ar-TPD-DRIFTS experiments showed the presence of CO bond to Pt sites and some carbonates (Fig. 9d). The CO_2 and H_2 desorption detected here is suggested to come from (i) decomposition of those carbonates that were not fully removed by evacuation and (ii) reaction of linear CO and (the support) OH groups at the metal-support interface in a WGS-like reaction as the reverse of reaction [7] shows. According to the literature [29,38] CO adsorbed on metal sites can interact with OH groups of the support to yield formate, which decomposes during TPD to CO_2 and H_2 if water is present, otherwise, the formate decomposes back to CO + OH. This formate decomposition was found to be enhanced by the presence of alkali additives. Thus, we should underline that our Pt sample is active in WGSR, and indeed, water desorbs even at higher temperatures than from the Ni samples during these TPD measurements.

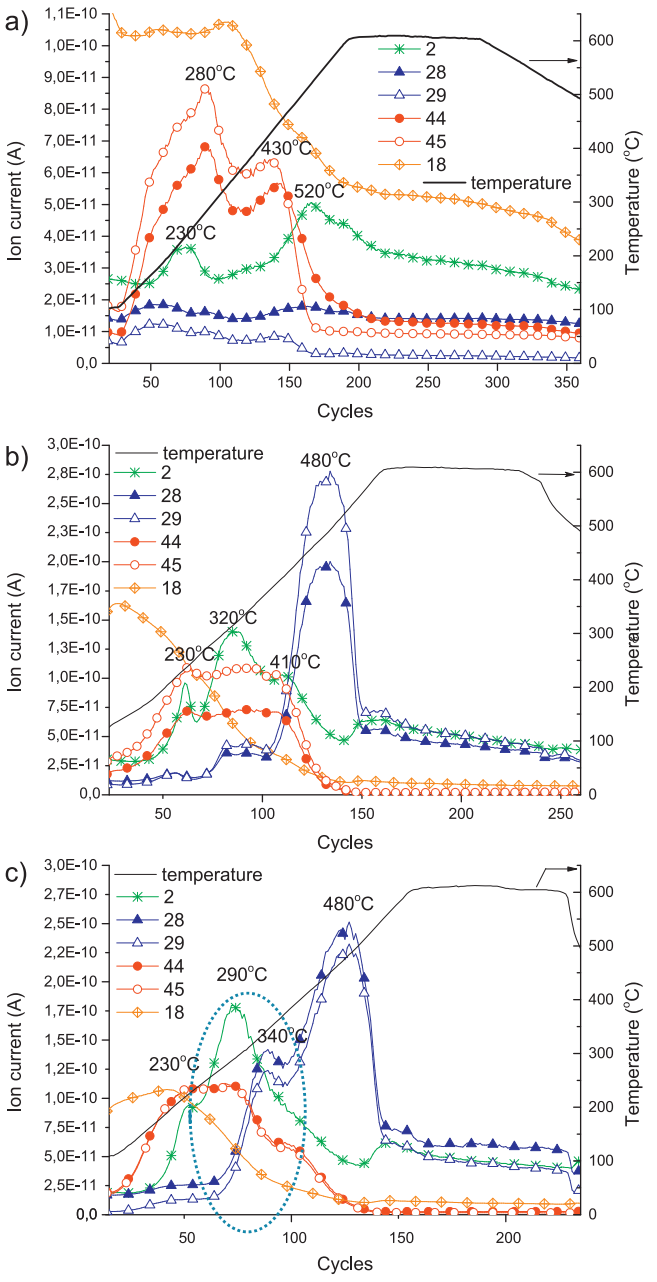

Fig. 12. TPD after dry reforming reaction in circulation system. (a) Zr8Pt1imp, (b) Zr8Ni1imp and (c) Zr6Ni3imp. Conditions: temperature ramp up to 600 °C with 10 °C/min, then 30 min isothermal part, *x* axis reflects time (1 MS cycle ~ 25.8 s), main peaks are signed with temperatures of maxima.

Going further to analyze the TPD results of the Ni samples, in the case of Zr8Ni1imp, labeled and unlabeled CO_2 (between 230 and 410 °C), H_2 (overlapping peaks with the largest maximum at 320 °C), and in the form of a large TPD peak, labeled and unlabeled CO was seen at 480 °C. On Zr6Ni3imp catalyst very similar TPD profile was obtained. The important difference is that CO desorbed in a small and a larger peak, and the smaller one at 340 °C was practically missing from the TPD spectrum of Zr8Ni1imp, furthermore, slightly more intense H_2 peaks were seen. We suppose that the first CO peak at 340 °C could originate from the conversion of highly reactive surface carbon, probably according to the $CH_{xads} + O_{ads}$ (or OH_{ads}) $\leftrightarrow CH_xO_{ads} + (H_{ads})$ reaction followed by the decoposition of this aldehyde-like (if $x = 2$) surface complex to CO and H_2 as was described in reactions [10,11] and also by Rozovskii et al. during spectroscopic study of surface compounds in methanol conversions

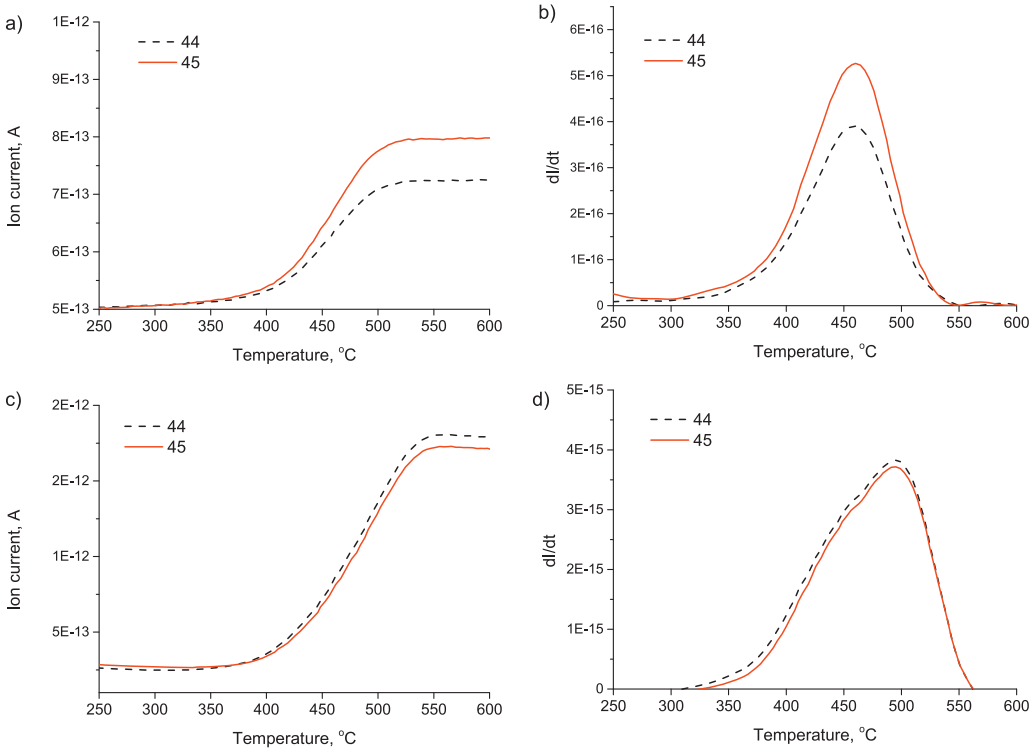

Fig. 13. TPO after TPD and DRM in circulation system. (a) Results on Zr8Ni1imp, (b) the corresponding derivated curves, (c) results on Zr6Ni3imp and (d) the corresponding derivated curves. Conditions: 200 mbar O_2, temperature ramp up to 600 °C with 10 °C/min, then 30 min isothermal part, m/e = 44 denotes CO_2, m/e = 45 denotes $^{13}CO_2$.

[39]. The high temperature CO peak observed in the TPD experiments may reflect the surface reaction between $O_{ads} + C_{ads} \rightarrow CO$, in which the final carbonate decomposition could take part as well. The remaining coke is removed only by oxygen in the following TPO.

Concerning the ratio of $^{13}C/^{12}C$ in the TPD spectra, we can suggest, that the desorbing C components contain more ^{13}C in the case of the first two samples (Fig. 12 curves a and b) than in the case of Zr6Ni3imp. It is expectable also from the DRM reaction since $^{13}CO_2$ conversion was seemingly higher on all the samples.

In Fig. 13, TPO curves of the carbon species that were not removed by the preceding TPD runs are depicted. CO_2 formation in the presence of 200 mbar oxygen was detected only on the Ni samples, the more on the Zr6Ni3imp. For a clearer view, the integral signal of CO_2 formation obtained in the closed loop circulation system was differentiated. According to the figure, the isotopic distribution of the CO_2 reflects the same trend as expected: the ratio of labeled and unlabeled CO_2 was about the same on the most active, Zr6Ni3imp sample, 0.142 mg ^{12}C, and 0.133 mg ^{13}C was removed from Zr6Ni3imp; while 0.053 mg ^{13}C and 0.039 mg ^{12}C was removed from Zr8Ni1imp. The TPO peak maximum was 460 °C for Zr8Ni1imp and 490 °C for the Zr6Ni3imp, reflecting that the less carbon was easier to remove.

All in all, Pt/ZrO_2 with its clear surface seem to be more promising catalyst for long runs, due to the effective sodium promotion, small Pt size and the strong interaction of Pt with the support. Most of the coke on the most active 3 wt%Ni/ZrO_2 did not influence the catalytic conversions and did not poison the sites.

4. Conclusions

In the present work, 1%Ni/ZrO_2 and 3%Ni/ZrO_2 and 1%Pt/ZrO_2 samples were prepared by impregnation technique in excess water and with the addition of $NaHCO_3$ base to act as catalyst promoter as well. Structural investigations were carried out by TEM, TPR, XRD, XPS, CO-chemisorption DRIFTS methods. The calcined and reduced fresh catalysts contained nanoparticles in the range of 2–20 nm, the Pt/ZrO_2 sample had the highest metal dispersion. The presence of sodium promoter influenced the catalysts to different extent: it induced the population of unique bridged CO sites during CO chemisorption DRIFTS measurements on all the samples and caused binding energy shift to lower values in the case of the highly dispersed Pt/ZrO_2 during XPS measurements. According to the TPR results, on the surface of 3%Ni/ZrO_2 most of Ni species is in strong interaction with the support and reduces at around 490 °C, while on 1%Ni/ZrO_2 this fraction of Ni species is less. By XPS Ni was found partially in hydroxide form after the in situ reduction. Temperature programmed DRITFS-DRM experiments were applied to investigate the adsorbed surface species during dry reforming conditions with special attention to the surface carbonate species as possible reaction participants. On Ni samples, intense and stable carbonate bands were detected while on Pt sample linear CO bound to Pt and weak carbonate bands were seen, which is tentatively explained by the difference in metal dispersion and distribution of Na promoter in the samples.

In the atmospheric catalytic tests in plug flow reactor no coke was deposited on Pt catalyst, presumably because at low temperature the carbonates/formates at the interface decompose easily (they cannot form in large amount, basically) and the active O or OH species produce CO from CH_x species very fast. The significant role of water gas shift activity (seen during the plug flow tests and TPD experiments) of negatively charged Pt keeps the surface carbon species hydrogenated and easy to be removed even at higher temperature.

On Ni samples coke formation took place, but most part of this carbon on 3%Ni/ZrO_2 sample must reside on the support, and leave the catalytically active Ni sites free. The carbonates do not decompose easily as in Pt catalysts (DRIFTS results) and so oxygen or OH species to oxidize surface carbon are less. CO_2 dissociation on Ni can provide the main source of active oxygen species at higher temperatures. However, it is tentatively suggested, that the oxidized

part of Ni surface, ($Ni(OH)_2$) and Na_2CO_3 species on the support in the vicinity of Ni participate in the active oxidant transport. The ideal Ni/Na ratio and distribution of Na species on the surface of 3%Ni/ZrO_2 makes this sample a much better catalyst than 1%Ni/ZrO_2, which is reflected in high and stable catalytic activity and its reduction properties. The slightly higher surface concentration of Na in 1%Ni/ZrO_2 decreases its activity and coking tendency as well.

Closed loop circulation system with $^{13}CO_2$ reactant at 50 mbar total pressure was applied to trace the fate of different carbon species during the reaction. In spite of the different structural results obtained for Ni and Pt samples, an overall mechanism for the start of reaction could be suggested that holds for all catalysts. First, CO_2 is activated as $^{13}CO_{2(gas)} \leftrightarrow {}^{13}CO_{ads} + O_{ads}$ and the $^{13}CO_{ads}$ immediately desorbs (appearance of ^{13}CO in the gas phase). At 350–400 °C, $^{12}CH_4$ dissociation happens and the surface C get oxidized by abundant active O species and desorbs as $^{12}CO_2$ together with the recombined H_2 molecules. Next, ^{12}CO appears in the gas phase because of the incomplete oxidation of surface carbon due to less amount of available surface oxygen species and because of the $^{12}CO_2 \leftrightarrow {}^{12}CO + O$ reversible transformation on the catalyst surface. Labeled methane can form from $^{13}CO + H_2$ or $^{13}CO_2 + H_2$ via surface methanation reaction that proceeds through $^{13}C_{ads}$ intermediate species probably as $^{13}CH_xO_{ads} + H_{ads} \leftrightarrow {}^{13}CH_4 + H_2O$. According to our isotope labeled measurements, common reaction intermediates do exist at 600 °C.

Acknowledgments

The authors are indebted for financial support of Era-Chemistry and the Hungarian National Research Fund (OTKA NN#107170). Yu Lou at the Technical University of Munich, Department of Chemistry is acknowledged for the thermodynamic equilibrium calculations and for providing us with the ZrO_2 supports. We thank Dr. Zsolt Kasztovszky (MTA EK) for the PGAA measurement.

References

[1] C. Papadopoulou, H. Matralis, X. Verykios, in: L. Guczi, A. Erdőhelyi (Eds.), Catalysis for Alternative Energy Generation, Springer Science + Business Media, New York, 2012, pp. 57–128.
[2] M.-S. Fan, A.Z. Abdullah, S. Bhatia, Chem. Cat. Chem. 1 (2009) 192–208.
[3] J.W. Han, C. Kim, J.S. Park, H. Lee, Chem. Sus. Chem. 7 (2014) 451–456.
[4] M.K. Nikoo, N.A.S. Amin, Fuel Proc. Techn. 92 (2011) 678–691.
[5] S. Sokolov, E.V. Kondratenko, M.M. Pohl, U. Rodemerck, Int. J. Hydrogen Energy 38 (2013) 16121–16132.
[6] L.M. Aparicio, J. Catal. 165 (1997) 262–274.
[7] M.C.J. Bradford, M.A. Vannice, J. Catal. 173 (1998) 157–171.
[8] A.S. Bobin, V.A. Sadykov, V.A. Rogov, N.V. Mezentseva, G.M. Alikina, E.M. Sadovskaya, T.S. Glazneva, N.N. Sazonova, M.Y. Smirnova, S.A. Veniaminov, C. Mirodatos, V. Galvitta, G.B. Martin, Top. Catal. 56 (2013) 958–968.
[9] N. Sun, X. Wen, F. Wang, W. Peng, N. Zhao, F. Xiao, W. Wei, Y. Sun, J. Kang, Appl. Surf. Sci. 257 (2011) 9169–9176.
[10] B.B. Baeza, C.M. Pedrero, M.A. Soria, A.G. Ruiz, U. Rodemerck, I.R. Ramos, Appl. Catal. B: Environ. 129 (2013) 450–459.
[11] S. Damyanova, B. Pawelec, K. Arishtirova, M.V.M. Huerta, J.L.G. Fierro, Appl. Catal. B: Environ. 89 (2009) 149–159.
[12] Y.Z. Chen, B.J. Liaw, W.H. Lai, Appl. Catal. A: Gen. 230 (2) (2000) 73–83.
[13] J. Wei, E. Iglesia, J. Catal. 224 (2004) 370–383.
[14] A. Yamaguchi, E. Iglesia, J. Catal. 274 (2010) 52–63.
[15] A. Horváth, G. Stefler, O. Geszti, A. Kienneman, A. Pietraszek, L. Guczi, Catal. Today 169 (2011) 102–111.
[16] E. Lovell, Y. Jiang, J. Scott, F. Wang, Y. Suhardja, M. Chen, J. Huang, R. Amal, Appl. Catal. A: Gen. 473 (2014) 51–58.
[17] L.F. Li, C. Xia, C.T. Au, B.S. Liu, Int. J. Hydrogen Energy 39 (2014) 10927–10940.
[18] C. Gennequin, M. Safariamin, S. Siffert, A. Aboukaïs, E. Abi-Aad, Catal. Today 176 (2011) 139–143.
[19] X. Junke, Z. Wei, W. Jihui, L. Zhaojing, M. Jianxin, Chin. J. Catal. 30 (2009) 1076–1084.
[20] A. Horváth, L. Guczi, A. Kocsonya, G. Sáfrán, V. La Parola, L.F. Liotta, G. Pantaleo, A.M. Venezia, Appl. Catal. A: Gen. 468 (2013) 250–259.
[21] L. Guczi, Gy. Stefler, O. Geszti, I. Sajó, Z. Pászti, A. Tompos, Z. Schay, Appl. Catal. A: Gen. 375 (2010) 236–246.
[22] A. Ballarini, F. Basile, P. Benito, I. Bersani, G. Fornasari, S. de Miguel, S.C.P. Maina, J. Vilella, A. Vaccari, O.A. Scelza, Appl. Catal. A: Gen. 433–434 (2012) 1–11.
[23] A.D. Ballarini, S.R. de Miguel, E.L. Jablonski, O.A. Scelza, A.A. Castro, Catal. Today 107–108 (2005) 481–486.
[24] Q.J. Chen, J. Zhang, Q.W. Jin, B.R. Pan, W.B. Kong, T.J. Zhao, Y.H. Sun, Catal. Today 215 (2013) 251–259.
[25] C. Zhang, Y. Li, Y. Wang, H. He, Environ. Sci Technol. 48 (2014) 5816–5822.
[26] J.H. Bitter, PhD thesis, University of Twente, Enschede, the Nederlands, 1997.
[27] F. Arena, F. Frusteri, A. Parmaliana, Appl. Catal. A: Gen. 187 (1999) 127–140.
[28] A. Kitla, O.V. Safonova, K. Föttinger, Catal. Lett. 143 (2013) 517–530.
[29] P. Panagiotopoulou, D.I. Kondarides, J. Catal. 260 (2008) 141–149.
[30] E.-M. Kock, M. Kogler, T. Bielz, B. Klotzer, S. Penner, J. Phys. Chem. C 117 (2013) 17666–17673.
[31] L.F. Liotta, G.A. Martin, G. Deganello, J. Catal. 164 (1996) 322–333.
[32] S. Haag, M. Burgard, B. Ernst, J. Catal. 252 (2007) 190–204.
[33] G.K. Reddy, S. Loridant, A. Takahashi, P. Delichére, B.M. Reddy, Appl. Catal. A: Gen. 389 (2010) 92–100.
[34] R.W. Stevens, R.V. Siriwardane, J. Logan, Energy Fuels 22 (2008) 3070–3079.
[35] M.A. Goula, A. Lemonidou, A.M. Efstathiou, J. Catal. 161 (1996) 626–640.
[36] J.M. Wei, B.-Q. Xu, J.-L. Li, Z.-X. Cheng, Q.-M. Zhu, Appl. Catal. A: Gen. 196 (2000) 167–172.
[37] A. Shamsi, C.D. Johnson, Catal. Today 84 (2003) 17–25.
[38] T. Shido, Y. Iwasawa, J. Catal. 141 (1993) 71–81.
[39] V.A. Matyshak, L.A. Berezina, O.N. Sil'chenkova, V.F. Tret'yakov, G.I. Lin, A.Y. Rozovskii, Kinet. Catal. 50 (2009) 255–263.

Please cite this article in press as: M. Németh, et al., Appl. Catal. A: Gen. (2015), http://dx.doi.org/10.1016/j.apcata.2015.04.006